Optical Materials 80 (2018) 143–148

Contents lists available at ScienceDirect

Optical Materials

journal homepage: www.elsevier.com/locate/optmat

Enhancement in fluorescence quantum yield of MEH-PPV:BT blends for polymer light emitting diode applications

K.M. Nimith*, M.N. Satyanarayan, G. Umesh

Department of Physics, National Institute of Technology Karnataka, Surathkal, PO Srinivasnagar, Mangalore- 575025, Karnataka, India

ARTICLE INFO

Keywords:
Conjugated polymer
Fluorescence quantum yield
MEH-PPV
Benzothiadiazole
Polymer light emitting diodes
Electroluminescence

ABSTRACT

We have investigated the effect of blending electron deficient heterocycle Benzothiadiazole (BT) on the photophysical properties of conjugated polymer Poly [2-methoxy-5-(2-ethylhexyloxy)-1,4-phenylenevinylene] (MEH-PPV). Quantum yield (QY) value has been found to increase from 37% for pure MEH-PPV to 45% for an optimum MEH-PPV:BT blend ratio of 1:3. This can be attributed to the efficient energy transfer from the wide bandgap BT (host) to the small bandgap MEH-PPV (guest). The FTIR spectrum of MEH-PPV:BT blended thin film indicates suppression of aromatic C-H out-of-plane and in-plane bending, suggesting planarization of the conjugated polymer chains and, hence, leading to increase in the conjugation length. The increase in conjugation length is also evident from the red-shifted PL spectra of MEH-PPV:BT blended films. Single layer MEH-PPV:BT device shows lower turn-on voltage than single layer MEH-PPV alone device. Further, the effect of electrical conductivity of PEDOT:PSS on the current-voltage characteristics is investigated in the PLED devices with MEH-PPV:BT blend as the active layer. PEDOT:PSS with higher conductivity as HIL reduces the turn on voltage from 4.5 V to 3.9 V and enhances the current density and optical output in the device.

1. Introduction

Since the first report on organic/polymer light emitting diodes [1,2], there have been continuous efforts to improve the device efficiency and lifetime by employing novel device architectures and synthesizing new efficient organic materials [3–12]. Organic semiconductors (OSCs) are well suited for thin, light-weight, flexible and large area flat panel displays and solar cells. Organic Light Emitting Diodes (OLEDs), Solar Cells, Sensors and Lasers are some of the explored applications of OSCs [13–15]. Polymer light-emitting diodes (PLEDs) are of particular interest since they can be fabricated by low temperature solution processing and scalable technologies, such as inkjet printing, on large area flexible substrates [16,17]. Recent applications of PLEDs include flexible displays, solid-state lighting and short-range indoor optical communication [18–20].

Efficient charge injection, balanced charge transport, exciton formation and recombination within the active layer are the basic processes involved in the operation of a PLED [21]. However, it is well documented in the literature that the magnitude of hole transport in OSCs are a few orders greater than that of electron mobility, which is hindered by omnipresent electron traps at 3.6 eV [22]. The imbalance of charge carrier transport in the OSCs invariably results in poor device efficiency and performance. This problem has been partly addressed by the design and synthesis of new materials with balanced charge carrier transport and, also, by blending active layer material with electron transport material [23]. A multilayer device includes hole injection layer (HIL), hole transport layer (HTL), electron blocking layer (EBL) on one side of the electroluminescent (EL) layer and, hole blocking layer (HBL), electron transport layer (ETL), electron injection layer (EIL) between the EL layer and the cathode. Such devices show improved device performance [24]. However, a serious problem in such multilayer devices is the dissolution of pre-deposited polymer layer by the solution for the subsequent layer [25]. Hence, there is great interest in fabricating few-layer devices using blended polymer materials with good device efficiency [26].

Poly [2-methoxy-5-(2′-ethylhexyloxy)-1,4-phenylene vinylene] (MEH-PPV), a well-investigated electroluminescent conjugated polymer and Benzothiadiazole (BT), an electron deficient small molecule, have been widely used in the field of organic optoelectronics [27,28]. Recently, Bidgoli et al. have explored the possibility of blending these materials and applying it as a single electroluminescent layer in the polymer light emitting diodes [29,30]. The motivation behind this was to balance the charge carrier mobilities within the active layer and thereby avoiding the complexity of multilayer device structure. They could observe a reduction in the turn on voltage and an increase in the lifetime of these devices. However, an extensive study of the photo-

* Corresponding author.
E-mail address: nimithkm@gmail.com (K.M. Nimith).

https://doi.org/10.1016/j.optmat.2018.04.046
Received 10 November 2017; Received in revised form 22 April 2018; Accepted 23 April 2018
Available online 01 May 2018
0925-3467/

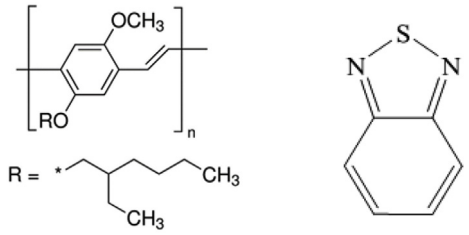

Fig. 1. Chemical structure of MEH-PPV and BT respectively (from Sigma-Aldrich website).

physical properties and different interaction mechanisms of these materials are still lacking in the literature. Here we report the enhancement in fluorescence quantum yield of MEH-PPV by the addition of BT. Fluorescence quantum yield (Φ_f), a measure of the efficiency of conversion of absorbed light into emitted light, is the key parameter for comparison of fluorophore efficiency. Relative fluorescence quantum yield can be easily measured using a UV–Vis spectrometer and a spectro-fluorometer.

2. Experimental details

MEH-PPV with a number averaged molecular weight (Mn) of 40000–70000 and with a polydispersity index (PDI) of around 6 and BT with a purity of 98% were purchased from Sigma Aldrich. Their chemical structures are shown in Fig. 1. Two varieties of PEDOT:PSS, one of conductivity (1 S/cm) grade (referred to as PEDOT:PSS1) and another with high-conductivity (> 200 S/cm) grade (PEDOT:PSS2) were also purchased from Sigma Aldrich. All these materials were used as received and without any further purification. Indium Tin Oxide (ITO) patterned glass substrates with sheet resistance of 15Ω/□ and thickness of 150 nm was sourced from Kintech, Taiwan, and used as the anode for the device fabrication. MEH-PPV and BT were separately dissolved in 1,2-dichorobenzene (DCB) to obtain solutions with a concentration of 1 mg/ml each. These two solutions were mixed together in different ratios to get appropriate weight percentages and subjected to the absorption and emission spectroscopy to investigate the effect of BT on the optical properties of MEH-PPV. Fluorescence quantum yields were calculated from the absorption and fluorescence spectra using a comparative method in which Fluorescein used as the standard.

UV–Vis absorption spectrum was recorded using Ocean Optics USB 4000 spectrophotometer with integration time of 30 ms. Fluorescence spectrum at room temperature was recorded using Horiba Jobin Yvon Fluoromax-4 spectrometer. Both the fluorescence reference standard and samples under the investigation were excited by light of wavelength 496 nm and the slit width of excitation and emission monochromators were kept 0.75 nm. FTIR spectrum of MEH-PPV and MEH-PPV:BT blend films were recorded by Perkin Elmer Frontier MIR spectrometer to investigate the structural changes and bond stretching or bending in MEH-PPV after blending with BT.

3. Results and discussions

3.1. Photo-physical studies of MEH-PPV and MEH-PPV:BT blends

Fig. 2 shows the normalized UV–Vis absorption curves for pure BT, pure MEH-PPV and for MEH-PPV:BT in a 1:3 blend in DCB solvent. The same curves were recorded for all other MEH-PPV:BT blend ratios (see the supporting information). The absorption spectrum shows characteristics absorption peak at 310 nm and 503 nm for solution of pure BT and MEH-PPV, respectively. The MEH-PPV:BT blend solution retains the absorption maxima at 310 nm, however, the absorption at 503 nm is much reduced. The absorption spectrum for 1:1 shows almost equal absorption for the constituent materials and is simply the linear combination of absorption spectrum of BT and MEH-PPV. As the weight

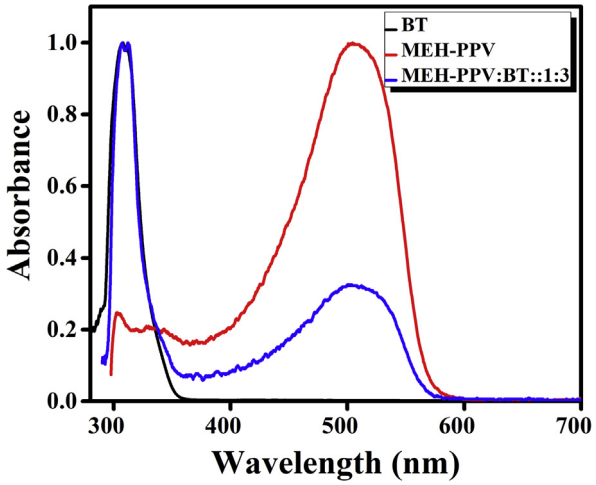

Fig. 2. Normalized UV–Vis absorption spectrum of MEH-PPV, BT and MEH-PPV:BT (1:3 ratio) solutions in DCB solvent.

percentage of MEH-PPV in the blend decreases, a similar reduction is seen in the absorbance. Optical bandgap of these materials was calculated by substituting the λ_{onset} value in the equation $E_g = \frac{1241.25}{\lambda_{onset}}$ eV, and found to be 3.55 eV and 2.18 eV for BT and MEH-PPV solutions, respectively. The calculated optical bandgap values are in good agreement with the values in the literature [31].

For very dilute solution (absorbance < 0.1) of BT, the excitation wavelength was 310 nm, corresponding to absorption maximum in UV–Vis, and the fluorescence emission (Fig. 3) was recorded from 325 nm to 600 nm. BT shows a narrow emission spectrum ranging from 350 nm to 450 nm with an emission maximum at 380 nm. MEH-PPV and MEH-PPV:BT solutions were excited with light at wavelength of 496 nm and the emission was recorded from 506 nm to 800 nm. Both the solutions show almost identical emission spectra without any shift in the peak wavelength. This suggests that blending has little effect on the shape of the PL spectrum and the optical band gap of MEH-PPV. Therefore, BT can be a good alternative for inducing the charge carrier balance in MEH-PPV without modifying the optical characteristics of MEH-PPV. Both MEH-PPV and MEH-PPV:BT blend solutions show a dominant peak at 569 nm and a shoulder at 610 nm, and their corresponding energy values are 2.18eV, 2.03eV respectively. Another shoulder peak at 668 nm (1.86eV) is barely visible. The energy difference between the three peaks are equal and it follows the usual vibronic progression [32]. A red shifted PL spectrum was obtained for both

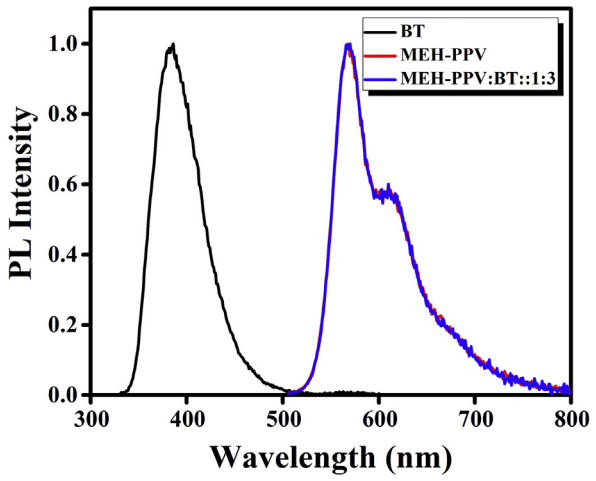

Fig. 3. Normalized fluorescence spectra of MEH-PPV, BT and MEH-PPV:BT (1:3 ratio) solutions in DCB solvent.

Table 1
Optical parameters obtained from the absorption and emission spectra.

Sample	Solvent	UV–Vis λ_{max} (nm)	PL λ_{max} (nm)	Stoke Shift λ_{PL}-λ_{UV} (nm)
MEH-PPV	DCB	503	570	67
BT	DCB	310	386	76
MEH-PPV:BT (1:3)	DCB	310, 503	568	65

Table 2
Fluorescence quantum yield values for different blend ratios of MEH-PPV with BT.

MEH-PPV:BT	1:0	1:1	1:2	1:3	1:4	1:5
QY (%)	37.48	40.79	42.96	45.54	38.67	38.26

MEH-PPV and MEH-PPV:BT blend (1:3 ratio) films compared to their solution state (see the supporting information).

The optical parameters obtained from the absorption and emission spectra are presented in Table 1.

Fluorescence quantum yield (Φ_f) is simply the ratio of number of photons emitted to the number of photons absorbed. Here we have adopted the commonly used comparative fluorescence quantum yield measurement technique taking fluorescein, dissolved in 0.1 M NaOH solution, as the reference standard whose QY value, taken from the literature is 0.95. Fluorescence quantum yield (Φ_f) is given by Refs. [33–35].

$$\Phi_{f,x} = \Phi_{f,st}\frac{F_x}{F_{st}}\frac{f_{st}}{f_x}\frac{n_x^2(\lambda_{em})}{n_{st}^2(\lambda_{em})} \quad (1)$$

Here F is the integral photon flux, f is the absorption factor, n is the refractive index (at the excitation wavelength) of the solvent and Φ_f is the quantum yield. The index x denotes the sample and the index st denotes the standard solution. F_x and F_{st} values were obtained by integrating the PL spectra over wavelength. The absorption factor is given by $f = 1 - 10^{-A(\lambda_{ex})}$, where $A(\lambda_{ex})$ is the absorbance at the excitation wavelength. Absorption factor can be considered as the absorbance value at the excitation wavelength for very dilute solution. All the solutions were taken in a quartz cuvette having a path length of 10 mm and were subjected to both absorption and fluorescence measurements. Here all the solution concentrations were restricted to get absorbance values less than 0.1 to ensure that self-absorption is negligible.

Here we substituted 1.335 and 1.551 for the refractive index value (at 589 nm) of the 0.1 M NaOH and DCB solvents, respectively. The slope values were extracted from the absorbance versus integrated fluorescence intensity graph (Fig. 4) and substituted in equation (1). The quantum yield values obtained for different blend ratios of MEH-PPV:BT are tabulated Table 2.

From the calculated QY values it is clear that the fluorescence quantum yield increases initially with increasing proportion of BT in the blend and attains a maximum QY value of 45% for MEH-PPV:BT blend ratio of 1:3. Further blending of BT into MEH-PPV resulted in reducing the QY value to 38% for blend ratio of 1:4 and more. Efficient energy transfer from a wide bandgap host to a small bandgap guest happens only when the emission spectrum of the host overlaps considerably with the absorption spectrum of the guest [6]. Since the emission spectrum of BT overlaps to some extent with the absorption spectrum of MEH-PPV, shown in Fig. 5, the energy transfer from the host BT to the guest MEH-PPV must be considered. The extent of overlap between the emission spectrum of BT and absorption spectrum of MEH-PPV was further improved when the blended liquid was cast into a solid film form (see the supporting information). This energy transfer can, in turn, result in the enhancement of fluorescence QY for MEH-PPV:BT blend.

Since MEH-PPV:BT:1:3 blend ratio resulted in maximum fluorescence QY, further characterizations and device fabrication were done using MEH-PPV:BT blend solution with 1:3 blend ratio only.

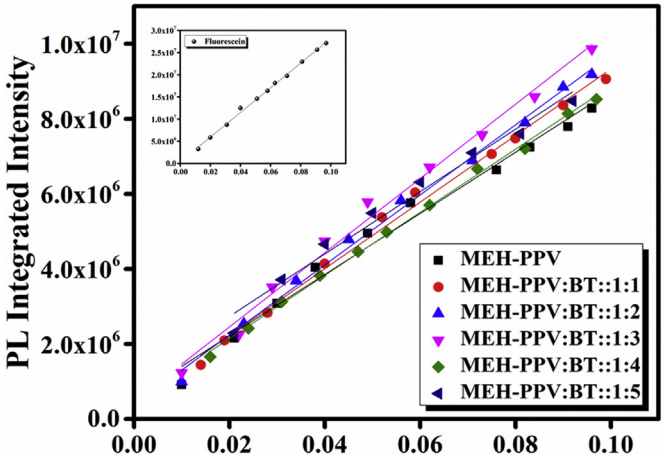

Fig. 4. Absorbance versus integrated fluorescence intensity graph for different blend ratios of MEH-PPV and BT. The same graph for fluorescein is shown in the inset. The absorbance values were recorded at a wavelength of 496 nm for both the sample and standard solutions.

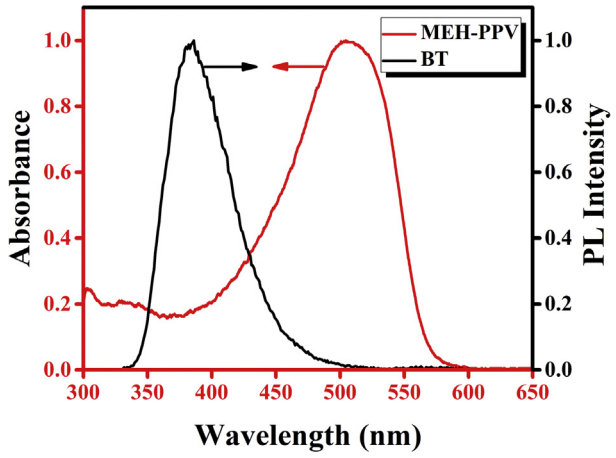

Fig. 5. Normalized absorption spectrum of MEH-PPV and PL emission spectrum of BT.

Infrared spectra of MEH-PPV and MEH-PPV:BT films were recorded by ATR method, from an upper limit 4000 cm^{-1} down to 650 cm^{-1}, to investigate whether there are any structural changes and bond stretching or bending in MEH-PPV after blending with BT. FTIR spectrum of the glass substrate was recorded as the reference. FTIR spectrum of MEH-PPV:BT blend film shown in Fig. 6 is similar to that of MEH-PPV except for the absence of vibrational frequencies at 727, 853, 1080, 1117, 1152, 2212, 3106 cm^{-1}. The absence of certain group frequencies implies that the blending results in reduced methylene-$(CH_2)_n$ – rocking and absence of aromatic C-H out-of-plane and in-plane bend [36]. The absence of aromatic C-H out-of-plane and in-plane bend in the MEH-PPV:BT blend can lead to planarization of the conjugated polymer chains and, thus, an increased conjugation length. The increase in conjugation length is further confirmed from the red-shifted PL spectra for MEH-PPV:BT blended films compared to MEH-PPV film [32,37]. In the PL spectra, full width at half maxima is 31 nm for MEH-PPV film and it reduces to 25 nm for MEH-PPV:BT blended films. The narrowing of the emission spectrum can be due to the dilution effects that decrease the conformational disorder in the blended films [32,38]. The conformational modification and the increased conjugation length can lead to an enhancement in the fluorescence quantum yield of MEH-PPV:BT thin films [38,39].

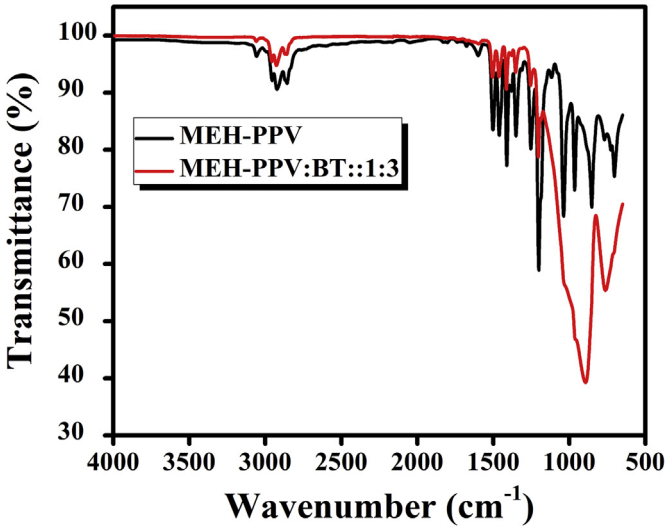

Fig. 6. FTIR spectra of MEH-PPV and MEH-PPV:BT thin films on glass substrate.

3.2. Polymer light emitting diodes (PLEDs) using MEH-PPV:BT blend

For the device fabrication, MEH-PPV and BT were separately dissolved in DCB at 5 mg/ml and blended together in the weight ratio 1:3. Single and multi-layer PLEDs were fabricated using this MEH-PPV:BT blend for the active layer since the blend ratio of 1:3 resulted in maximum fluorescence quantum yield. The device structure and the energy level diagram of the materials used in the devices are shown in Fig. 7. The blended solution was spin cast at a speed of 2000 rpm for 30 s. The amorphous nature of the MEH-PPV and MEH-PPV:BT blend films were confirmed by X-ray diffraction (XRD) and is presented in the supporting information. Active layer thickness of 100 nm was obtained by step height measurement of MEH-PPV:BT film using Atomic Force Microscope (AFM), in tapping mode (Bruker- Dimension Icon). Several multilayer devices were fabricated using PEDOT:PSS, of two different conductivities, as HIL and its effect on the device performance was investigated. The two PEDOT:PSS solutions were spin cast at 2000 rpm for 30 s yielding films of thickness 20 nm for PEDOT:PSS1 and 60 nm for PEDOT:PSS2, respectively. Aluminum film of thickness 120 nm was deposited as the cathode by thermal evaporation at a vacuum level of 5×10^{-6} mbar.

The current density-voltage characteristics of the devices, were recorded under ambient conditions just after the fabrication. Fig. 8 indicates that the high conductive PEDOT:PSS film works as a good hole injection layer and drastically reduces the turn on voltage, thereby increasing the current density in the devices. The turn on voltage for devices with high conductivity PEDOT:PSS2 is 3.9 V where as that of devices with lower conductivity PEDOT:PSS1 is 4.5 V. Clearly, the high conductivity PEDOT:PSS film plays the role of a good HIL. The J-V characteristics of MEH-PPV single layer device shows a higher turn on voltage (12 V) than the MEH-PPV:BT (1:3) single layer device (9 V).

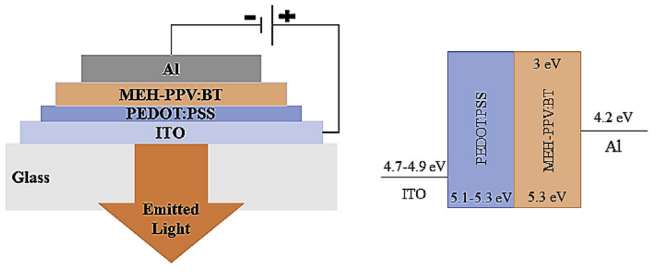

Fig. 7. Device structure and energy level diagram of multilayer PLEDs with MEH-PPV:BT as active layer.

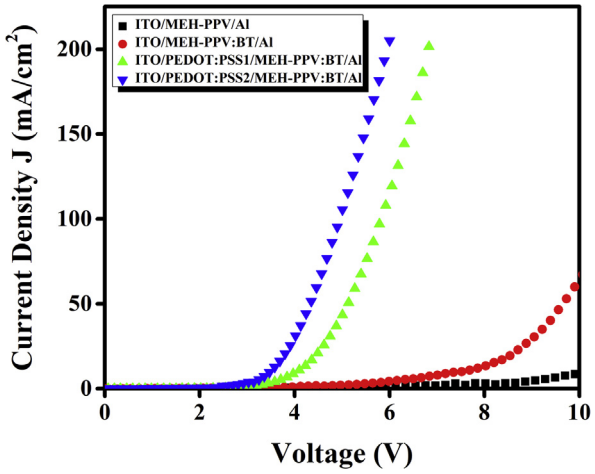

Fig. 8. Current density-voltage (J–V) characteristics of MEH-PPV:BT (1:3) blend devices with and without PEDOT:PSS film of different conductivities as HIL. J-V characteristics of MEH-PPV alone device is also shown for comparison.

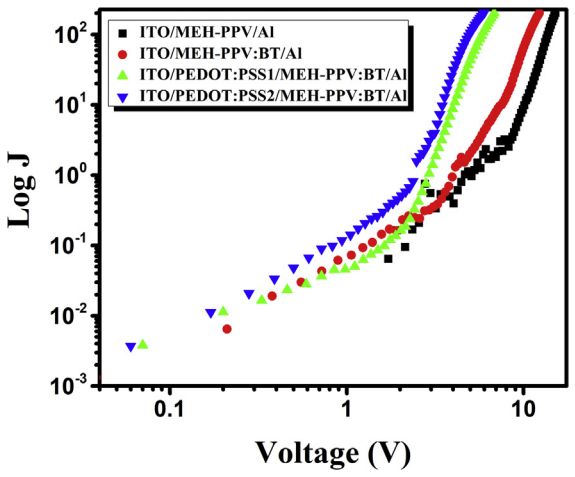

Fig. 9. Logarithmic plot of current density-voltage (J–V) characteristics of MEH-PPV:BT blend (1:3 ratio) devices with and without PEDOT:PSS as HIL.

The logarithmic (J-V) plot (Fig. 9) for single layer MEH-PPV:BT blend devices shows three distinct linear regions conforming to a power law behaviour ($J \alpha V^{k+1}$) [29]. At low voltages current injection mechanism is dominated by ohmic injection having a slope value of 0.90. At intermediate voltages, the conduction mechanism changes from ohmic to space charge limited (SCLC) type, with a slope value of 1.50. SCLC is exhibited by low-mobility semiconductor materials when the injected charge density is far greater than the intrinsic free carrier density. As the voltage increases further, the k value also increases to 4.98, signifying the domination of trap charge limited conduction (TCLC). Multilayer devices, having PEDOT:PSS and MEH-PPV:BT layers, also exhibit a similar behaviour with three distinct linear regions. Slope values of 0.94, 1.96 and 6.08 were obtained for devices with PEDOT:PSS1 and 1.05, 1.6 and 6.13 for devices with higher conductivity PEDOT:PSS2 layer as HIL.

In order to estimate the surface roughness of the PEDOT:PSS films, the morphology of the films have been studied using AFM. The AFM images (Fig. 10) of PEDOT:PSS films, yield a surface roughness rms value (Rq) of 2.85 nm for PEDOT:PSS2 and 3.48 nm for PEDOT:PSS1. Although the AFM images of PEDOT:PSS2 film looks highly granular, NanoScope software analysis shows lower surface roughness for PEDOT:PSS2. Therefore the high conductive PEDOT:PSS2 can form a better interface with the MEH-PPV:BT emissive layer and, hence, enhances the charge injection into MEH-PPV:BT layer.

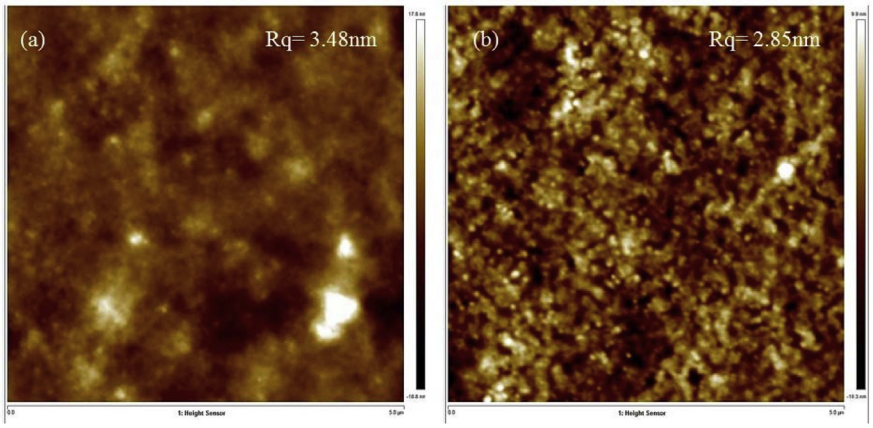

Fig. 10. Surface roughness of (a) PEDOT:PSS1 (b) PEDOT:PSS2 thin films on glass substrates using AFM at a scan area of 5 μm × 5 μm.

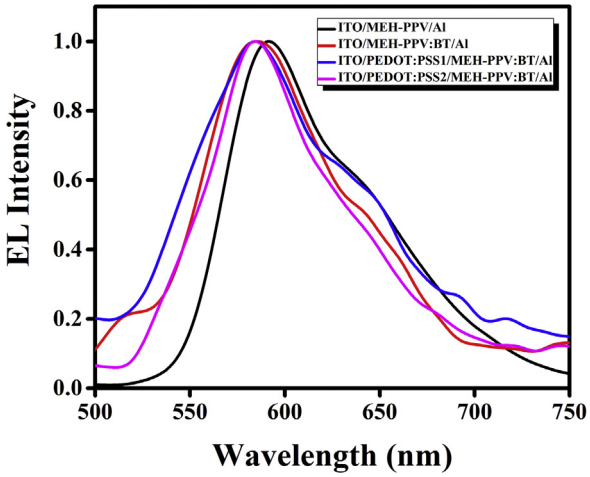

Fig. 11. Normalized electroluminescence (EL) spectra of the devices with MEH-PPV alone and MEH-PPV:BT:1:3 blend as active layers. EL recorded at a bias voltage corresponding to the current density of ~100 mA/cm^2 for all the devices (5 V, 6 V, 11 V and 14 V, respectively for ITO/MEH-PPV/Al, ITO/MEH-PPV:BT/Al, ITO/PEDOT:PSS1/MEH-PPV:BT/Al, ITO/PEDOT:PSS2/MEH-PPV:BT/Al devices).

Fig. 11 shows the electroluminescence (EL) spectrum of the devices with MEH-PPV alone and MEH-PPV:BT blend, as active layer. The EL spectra were recorded over a wavelength range 300–800 nm using a spectrometer (Flame, Ocean Optics). The EL spectrum was trimmed between 500 and 750 nm to avoid the noise present in it. All the devices exhibit a broad EL ranging from a wavelength of 525 nm–725 nm. Emission maxima occurs close to 591 nm wavelength for MEH-PPV based devices and at 586 nm for MEH-PPV:BT based devices. The small blue shift in the emission maxima of MEH-PPV:BT devices can be due to the interaction between MEH-PPV and BT. It is well documented that the PL spectrum of the fluorescent molecules shows a red shift in the solid state compared to the respective solution state. The PL spectrum resembles the EL spectrum for these materials. The PL spectrum of BT solution shows the emission maxima at 386 nm and is expected to exhibit a red shifted EL emission in film form. Hence, the strong EL emission at 586 nm from the MEH-PPV:BT device may be ascribed to MEH-PPV only [40].

The optical output measurement shows that same current density (~100 mA/cm^2) resulted in higher number of photons (integration from 400 nm to 700 nm) for single layer MEH-PPV:BT blended device (1.69×10^{10}) than the single layer MEH-PPV alone device (8.23×10^{9}). From the optical and electrical characterizations, it is clear that blending MEH-PPV and BT together and applying it as an active layer resulted in a lower turn-on voltage and better device efficiency than MEH-PPV alone device. Further, multilayer device with PEDOT:PSS as HIL improves the optical output due to better hole injection. Device with high conductivity PEDOT:PSS2 as HIL shows improved optical output and large number of photons (2.61×10^{10}) than the device with lower conductive PEDOT:PSS1 (2.49×10^{10}).

4. Summary and conclusions

Fluorescence quantum yield (Φ) measurement reveals that the addition of BT into MEH-PPV resulted in an enhancement in the fluorescence efficiency. A maximum quantum yield of 45% obtained for an optimum blend ratio of 1:3 for MEH-PPV:BT. This can be attributed to the efficient energy transfer from the wide bandgap host to the small bandgap guest. FTIR spectra revealed the suppression of aromatic C-H out-of-plane and in-plane bending in the MEH-PPV:BT blend. This leads to the planarization of the conjugated polymer chains and increased conjugation length. Single layer MEH-PPV:BT device shows lower turn on voltage and higher optical output than single layer MEH-PPV alone device. Use of high conductivity PEDOT:PSS film as HIL enhances the charge injection into the active polymer and reduces the turn on voltage of the device. AFM image shows a smoother surface for the high conductivity PEDOT:PSS films and therefore forms a better interface between HIL and active polymer layer resulting in enhanced charge injection. Blending of MEH-PPV and BT does not affect the photo-physical properties of MEH-PPV and the EL originates only from MEH-PPV. Therefore, BT is seen to be a good candidate to induce balanced charge carrier transport and obtain emission enhancement in MEH-PPV based PLEDs, with less device complexity.

Acknowledgements

A portion of this research was performed using facilities at CeNSE, funded by Ministry of Electronics and Information technology (MeitY), Govt. of India, and located at the Indian Institute of Science, Bengaluru. KMN is grateful to N.I.T.K., Surathkal, for granting him a research fellowship.

Appendix A. Supplementary data

Supplementary data related to this article can be found at http://dx.doi.org/10.1016/j.optmat.2018.04.046.

References

[1] C.W. Tang, S.A. Vanslyke, Organic electroluminescent diodes, Appl. Phys. Lett. 51 (1987) 913–915.
[2] J.H. Burroughes, et al., Light-emitting diodes based on conjugated polymers, Nature

347 (1990) 539–541.
[3] D.L. Sivco, A.Y. Cho, G.J. Zydzik, Highly Efficient Lig Ht-Emitting Diodes with Microcavities vol. 265, (1994).
[4] V. Bulovic, G. Gu, P.E. Burrows, S.R. Forrest, M.E. Thompson, Transparent light-emitting devices, Nature 380 (1996) 29.
[5] S.R. Forrest, et al., The stacked OLED (SOLED): a new type of organic device for achieving high-resolution full-color displays, Synth. Met. 91 (1997) 9–13.
[6] M.A. Baldo, et al., Highly efficient phosphorescent emission from organic electroluminescent devices, Nature 395 (1998) 151–154.
[7] S. Reineke, et al., White organic light-emitting diodes with fluorescent tube efficiency, Nature 459 (2009) 234–238.
[8] A. Endo, et al., Thermally activated delayed fluorescence from Sn4 + -Porphyrin complexes and their application to organic light emitting diodes - a novel mechanism for electroluminescence, Adv. Mater. 21 (2009) 4802–4806.
[9] S. Reineke, M. Thomschke, B. Lussem, K. Leo, White organic light-emitting diodes: status and perspective, Rev. Mod. Phys. 85 (2013) 1245–1293.
[10] Q.D. Ou, et al., Extremely efficient white organic light-emitting diodes for general lighting, Adv. Funct. Mater. 24 (2014) 7249–7256.
[11] J.K. Kim, et al., Origin of white electroluminescence in graphene quantum dots embedded host/guest polymer light emitting diodes, Sci. Rep. 5 (2015) 1–11.
[12] M.Y. Wong, Recent advances in polymer organic light-emitting diodes (PLED) using non-conjugated polymers as the emitting layer and contrasting them with conjugated counterparts, J. Electron. Mater. (2017), http://dx.doi.org/10.1007/s11664-017-5702-7.
[13] A. Dickinson, T, J. White, J.S. Kauer, Lasing from conjugated polymer Microcavities.pdf, Nature 382 (1996) 695–697.
[14] Hu, W. Organic Electronics II Organic Photovoltaics Physics of Organic Semiconductors Physical and Chemical Aspects of Organic Electronics.
[15] X. Dai, et al., Solution-processed, high-performance light-emitting diodes based on quantum dots, Nature 515 (2014) 96–99.
[16] R.H. Friend, et al., Electroluminescence in conjugated polymers, Natalia 397 (1999) 121–128 www.nature.com.
[17] H. Zheng, et al., All-solution processed polymer light-emitting diode displays, Nat. Commun. 4 (2013) 1971.
[18] G. Gustafsson, et al., Flexible light-emitting-diodes made from soluble conducting polymers, Nature 357 (1992) 477–479.
[19] M.S. White, et al., Ultrathin, highly flexible and stretchable PLEDs, Nat. Photon. 7 (2013) 811–816.
[20] P.A. Haigh, et al., Visible light communications: real time 10 Mb/s link with a low bandwidth polymer light-emitting diode, Optic Express 22 (2014) 2830.
[21] X.-Y. Deng, Light-emitting devices with conjugated polymers, Int. J. Mol. Sci. 12 (2011) 1575–1594.
[22] H.T. Nicolai, et al., Unification of trap-limited electron transport in semiconducting polymers, Nat. Mater. 11 (2012) 882–887.
[23] P. Cea, et al., A blended layer MEH-PPV electroluminiscent device incorporating a new electron transport material, Mater. Sci. Eng. C 22 (2002) 87–89.
[24] N. Prasad, et al., Improving the performance of MEH-PPV based light emitting diode by incorporation of graphene nanosheets, J. Lumin. 159 (2015) 166–170.
[25] C. Newby, J.K. Lee, C.K. Ober, The solvent problem: redissolution of macromolecules in solution-processed organic electronics, Macromol. Res. 21 (2013) 248–256.
[26] D. Abbaszadeh, et al., Elimination of charge Carrier trapping in diluted semiconductors, Nat. Mater. 15 (2016) 628–633.
[27] P. Herguth, X. Jiang, M.S. Liu, A.K. Jen, Highly Efficient Fluorene- and Benzothiadiazole-based Conjugated Copolymers for Polymer Light-emitting Diodes, (2002), pp. 6094–6100.
[28] Y. Tao, et al., Synthesis and characterization of efficient luminescent materials based on 2, 1, 3-benzothiadiazole with carbazole moieties, Synth. Met. 161 (2011) 718–723.
[29] M.M. Bidgoli, M. Mohsennia, F.A. Boroumand, A.M. Nia, Optoelectronic characteristics of MEH-PPV + BT blend thin films in polymer light emitting diodes, Semicond. Sci. Technol. 30 (2015) 065016.
[30] M. Mohsennia, M.M. Bidgoli, F.A. Boroumand, A.M. Nia, Electrically conductive polyaniline as hole-injection layer for MEH-PPV: BT based polymer light emitting diodes, Mater. Sci. Eng. B 197 (2015) 25–30.
[31] E. Xu, et al., The synthesis and properties of novel pi -conjugated 2,1,3-benzothiadiazole oligomers, Dyes Pigments 80 (2009) 194–198.
[32] V.S. Reddy, A. Dhar, Ã. Optical and charge Carrier transport properties of polymer light emitting diodes based on MEH-PPV, Phys. B Phys. Condens. Matter 405 (2010) 1596–1602.
[33] C. Würth, M. Grabolle, J. Pauli, M. Spieles, U. Resch-genger, Relative and absolute determination of fluorescence quantum yields of transparent samples, Nat. Protoc. 8 (2013) 1535–1550.
[34] Christian Würth, Markus Grabolle, Jutta pauli, Monika Spieles, U. R.-G. Comparison of methods and achievable uncertainties for relative and absolute measurements of photoluminescence quantum yields, Anal. Chem. 83 (2011) 3431–3439.
[35] A.M. Brouwer, Standards for photoluminescence quantum yield measurements in solution (IUPAC Technical Report), Pure Appl. Chem. 83 (2011) 2213–2228.
[36] J. Coates, Interpretation of infrared spectra, a practical approach interpretation of infrared spectra, a practical approach, Encycl. Anal. Chem (2000) 10815–10837, http://dx.doi.org/10.1002/9780470027318.
[37] S. Giri, C.H. Moore, J.T. Mcleskey, P. Jena, Origin of red shift in the photoabsorption peak in MEH − PPV polymer, J. Phys. Chem. C 118 (2014) 13444–13450.
[38] A. Marletta, V.C. Gonçalves, D.T. Balogh, Effect of temperature on emission of MEH-PPV/PS solid-state solution, J. Lumin. 116 (2006) 87–93.
[39] I. Botiz, et al., Enhancing the photoluminescence emission of conjugated MEH-PPV by light processing, ACS Appl. Mater. Interfaces 6 (2014) 4974–4979.
[40] M. Berggren, et al., Light-emitting-diodes with variable colors from polymer blends, Nature 372 (1994) 444–446.